Int. J. Electrochem. Sci., 14 **(2019)** 6366 – 6375, doi: 10.20964/2019.07.04

International Journal of
ELECTROCHEMICAL
SCIENCE
www.electrochemsci.org

Electrochemical Study, Structural Characterization and Antimicrobial Activity of Silver and Copper Oxide (CuO) Nanoparticles Synthesized by a Green Method Using L-ascorbic Acid and Chitosan

M.E. Vázquez[1], *J.R. López*[1], *D. Medina-Rodelo*[1], *M. Jiménez-Edeza*[1], *G.M. Castañeda-Ruelas*[1], *A.M. López*[1], *J.M. Herrera-Ramírez*[2], *P.F. Méndez*[1,*]

[1] Facultad de Ciencias Químico Biológicas, Universidad Autónoma de Sinaloa, Cd. Universitaria, Av. de las Américas y Josefa Ortiz S/N, 80000, Culiacán, Sinaloa, México.
[2] Centro de Investigación en Materiales Avanzados, Laboratorio Nacional de Nanotecnología, Miguel de Cervantes 120, 31136, Chihuahua, Chih., México.
[*]E-mail: pmendez@uas.edu.mx

Received: 15 January 2019 / *Accepted:* 24 March 2019 / *Published:* 10 June 2019

An economical and facile green method for the synthesis of nanoparticles was employed to prepare silver and copper oxide nanostructures using L-ascorbic acid as the reducing agent. The effect of pH on the resulting nanoparticles was studied. The results show that with increased solution pH, the nanoparticles are larger, in the range of 19-50 nm for silver and 5-30 nm for copper oxide. The interplanar distances and selected area electron diffraction patterns show that both kinds of nanoparticles are highly crystalline. The silver nanocrystals present face-centered cubic structure, while the copper oxide nanoparticles have monoclinic structure. These results agree with those obtained in the electrochemical study since the peaks of the oxidation-reduction pairs correspond to Ag^0/Ag^+ for silver and Cu^0/Cu^+ and Cu^+/Cu^{2+} for copper. Finally, the smallest copper oxide nanoparticles presented high antibacterial activity comparable with that of a conventional drug.

Keywords: Cyclic voltammetry, TEM, UV-Vis spectrophotometry, Silver nanoparticles, Copper oxide nanoparticles, Green synthesis, Antimicrobial activity

1. INTRODUCTION

A nanoparticle in any of its presentations (nanopowder, nanocluster or nanocrystal) is a particle with a diameter between 1 and 100 nm. Nanoparticles are important technological and scientific materials that are being explored in various fields, such as medicine, electronics, food, fuel cells, solar cells, space, coatings, paints, water treatment, etc.; their importance lies in the difference between

these materials and bulk materials due to the nanoparticle properties, which depend to a great extent on their size and shape. Nanoparticles can be classified into different types according to their size, morphology, physical and chemical properties. Some such types include carbon-based nanoparticles, ceramic nanoparticles, metal nanoparticles, semiconductor nanoparticles, polymeric nanoparticles and lipid-based nanoparticles. In particular, metallic and semiconductor nanoparticles have gained great popularity in recent years due to their wide fields of application, such as biomedical applications [1] for the release of drugs, sensor devices or cancer treatment; paints [2]; electronics [3]; and antimicrobial functions [4], among others. In this sense, silver nanoparticles (AgNPs) and copper oxide nanoparticles (CuONPs) are the most used and have been applied in many consumer products owing to their excellent properties, especially antimicrobial activity and biochemical detection. However, their synthesis usually involves a chemical reduction reaction where toxic chemicals are used. For that reason, more sustainable methods, which are known as "green synthesis", have been proposed. These methods use green materials that are generally found in nature, mainly in plant extracts [5, 6], or other environmentally friendly compounds, such as ascorbic acid or chitosan, which can work as reducing and/or capping agents [7]. In this work, an economical and reproducible green method to synthesize AgNPs and CuONPs based on the use of simple equipment and few non toxic reagents was developed. This research is supported by measurements of the antimicrobial activity of the nanoparticles, as well as electrochemical, optical and structural analysis.

2. MATERIALS AND METHODS

2.1 Materials

All materials were reagent grade and were used as received. Copper nitrate (99%), silver nitrate (99.3%), sodium citrate (99.3%) and nitric acid (70%) were purchased from Fermont. L-ascorbic acid (99.9%), acetic acid (99%) and sodium hydroxide (96%) were purchased from ICR, and chitosan with medium molecular weight was purchased from Sigma Aldrich.

2.2 Synthesis of nanoparticles

2.2.1 Synthesis of silver nanoparticles

The synthesis of silver nanoparticles was carried out using a procedure similar to that reported by Suriati et al. [8]. Then, 0.1 ml of 0.1 M silver nitrate solution was added to 10 ml of a solution containing 8 ml of $6x10^{-4}$ M ascorbic acid and 2 ml of $3x10^{-3}$ M sodium citrate at room temperature; the mixture was kept in constant agitation until a change in color from transparent to black was observed. Once the aforementioned reagents were mixed, the mixture was kept at 100 °C for 2 h using a reflux system. The synthesis was carried out at different pH values (3, 7 and 10) to evaluate the effect of pH on the size and morphology of the nanoparticles.

2.2.1 Synthesis of copper oxide (CuO) nanoparticles

The procedure reported by Zain et al. [5] was modified to synthesize CuONPs: 10 ml of 0.2 M copper nitrate solution was mixed with 4 ml of 1% w/v chitosan and 4 ml of 1 M ascorbic acid. Before the experiment, the solutions were bubbled with nitrogen for 5 min; the pH was adjusted to 3, 7 and 10 using sodium hydroxide and/or nitric acid to evaluate the effect of pH on the size and morphology of the nanoparticles. After mixing, the solutions were stirred at 60 °C for 30 min and finally at 100 °C for 2 h using a reflux system.

2.3 Electrochemical, optical and structural characterization

Electrochemical tests were performed in a PAR 263A potentiostat-galvanostat with a three-electrode cell using platinum, silver wire and Ag/AgCl as the working electrode, counter electrode and reference electrodes, respectively. A 0.3 M HCl solution was used as the electrolyte with a scan rate of 100 mV/s. The nanoparticles were characterized by ultraviolet-visible (UV-Vis) spectrophotometry in a UNICO 2802 instrument. The microstructural characterization of nanoparticles was carried out by scanning electron microscopy (SEM) using a JEOL JSM7401F field emission microscope operated at 25 kV. Transmission electron microscopy (TEM) was performed using a HITACHI HT7700 microscope operated at 80-100 kV. High-resolution transmission electron microscopy (HRTEM) was performed using a JEOL JEM-2200FS+CS microscope operated at 200 kV. Selected area electron diffraction (SAED) patterns were acquired using this microscope with a camera length of 80-100 cm and an image resolution of 150 pixels/inch. For TEM and HRTEM analysis, samples were prepared in copper (for Ag samples) and nickel (for CuO samples) grids by the dropping method and allowed to dry under a tungsten filament lamp for 5 min.

2.4 Antimicrobial activity

The antimicrobial activity of the AgNP and CuONP solutions was tested with both Gram-negative (*Escherichia coli* ATCC 25922) and Gram-positive (*Staphylococcus aureus* ATCC 29213) bacteria according to the agar well diffusion method. Briefly, a 100 µl aliquot of bacterial suspension ($1x10^8$ UFC/ml) was uniformly spread onto the surface of Muller-Hinton agar. Then, the wells were punched with a sterile tip (6 mm). The wells were filled with 50 µl of nanoparticle solution, and the plates were incubated at 35 ± 2 ºC for 24 h. A ceftriaxone (30 µg/ml) disk was used for quality control. The antimicrobial activity was expressed as the growth-inhibition zone diameter (cm) and was calculated by using the following formula: inhibition zone = total diameter of growth-inhibited zone minus diameter of the well. The test was performed in triplicate.

All data were processed by ANOVA with Tukey´s and Dunnett's tests using Minitab software (version 18.0) to determine the significance of the difference between means. A $p < 0.05$ value was considered statistically significant.

3. RESULTS AND DISCUSSION

3.1 Optical characterization

Figure 1a shows the UV-Vis spectra of AgNPs synthesized at pH 7 and 10, where surface plasmon resonance (SPR) characteristic of this material was observed at 409 nm for both systems. The maximum absorption peak for AgNPs is typically reported in the region of 350–450 nm [9]. Shifts or shape changes in the SPR band and changes in absorbance values (increases or decreases) can be related to changes occurring in the solution; in this case, it is expected that the nanoparticles obtained at pH 10 will present a larger size interval than those synthesized at pH 7. It was not possible to obtain the characteristic peak for samples synthesized at pH 3 because this pH value does not favor the formation and growth of nanoparticles. This effect can be attributed to the stability of silver nanoparticles, which depends on the working solution pH; the nanoparticle growth can be stopped. These nanoparticles are unstable in acidic media and can be formed easily in basic media, where hydroxylic groups are predominant, as reported by Hussain et al. [10].

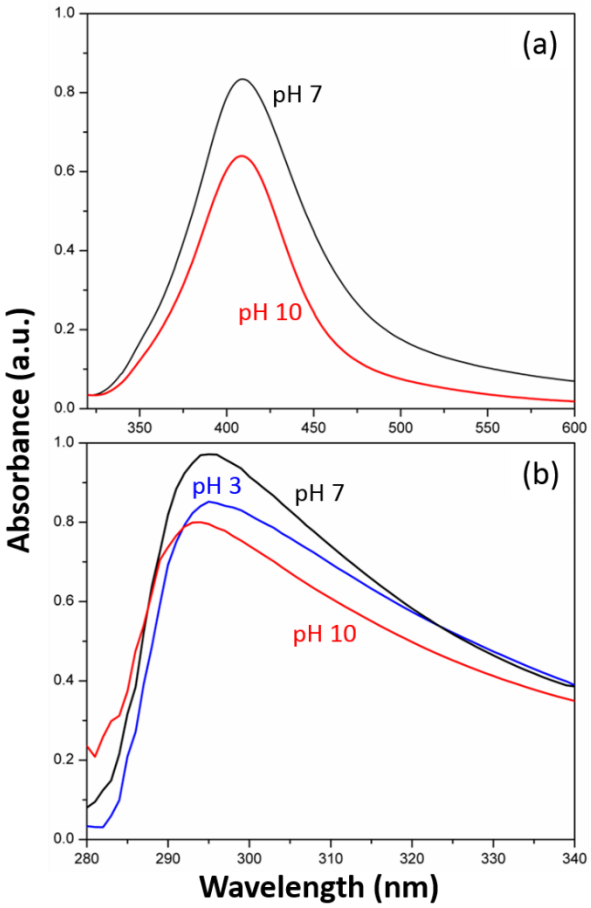

Figure 1. UV–Vis absorption spectra obtained for (a) AgNPs and (b) CuONPs at different pH values.

On the other hand, copper oxide nanoparticles were obtained for all the pH values studied, with an absorbance peak of 295 nm for pH 3 and pH 7 and a peak of 294 nm for pH 10, which is the characteristic band of CuO [11, 12]. The UV-Vis spectra are very similar in shape and λ_{max} value, but

the pH affects the width of the absorption peaks. This effect indicates that the size and distribution of nanoparticles is affected by pH, as seen in the structural characterization results.

3.2 Structural characterization

SEM, TEM and HRTEM analysis revealed that both the silver and copper oxide nanoparticles are nearly spherical in shape, as shown in Figures 2 and 3, respectively. For both kinds of nanoparticles, the higher the pH is, the larger the particle size. Indeed, the average particle size of AgNPs is 29.9 ± 10.8 nm and 43.4 ± 13.2 nm at pH 7 and pH 10, respectively, while the average size of CuONPs is 1.7 ± 0.3, 2.6 ± 0.2 and 5.1 ± 0.7 nm for a pH of 3, 7 and 10, respectively. Figure 2 shows AgNPs synthesized at pH 10. Figure 2a shows an SEM image of AgNPs, whose composition was confirmed by energy-dispersive spectroscopy (EDS) coupled to a microscope (inset in Figure 2a). Figure 2b presents a TEM micrograph of a set of Ag nanoparticles, showing that their shape is essentially spherical. Figure 2c displays a representative HRTEM image of a silver nanoparticle, where the interplanar distance was calculated to be 0.252 nm (inset in Figure 2c), which matches the {1,1,1} lattice planes of the face-centered cubic (fcc) structure of silver. Figure 2d shows the SAED pattern indexed with the help of Process Diffraction software [13]; the diffraction rings can be indexed to the (1,1,1), (2,0,0), (2,2,0) and (3,1,1) planes of the silver fcc structure. These results indicate that the AgNPs possess high crystallinity.

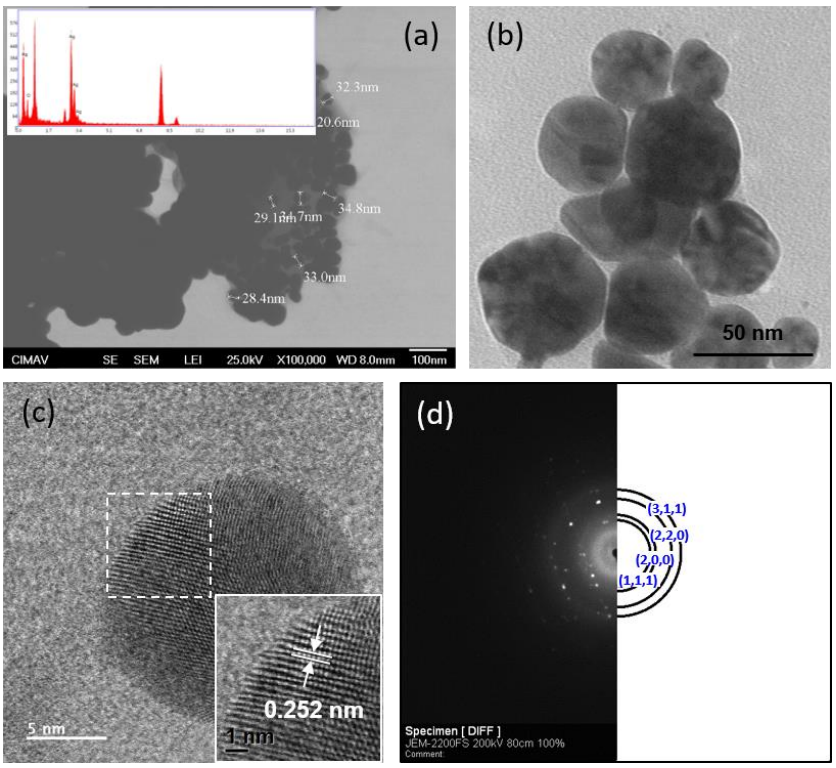

Figure 2. Ag nanoparticles synthesized at pH 10: (a) SEM and EDS analysis, (b) TEM micrograph showing several Ag nanoparticles, (c) HRTEM image of an Ag nanoparticle, (d) indexed SAED pattern.

Figure 3 presents images of CuONPs synthesized at pH 10, which are similar to Ag nanoparticles. Figure 3a shows an SEM image of a CuONP cluster; the composition of the nanoparticles was confirmed by EDS (inset in Figure 3a). Figure 3b presents a TEM micrograph of a set of spherical CuO nanoparticles, which are surrounded by a layer of chitosan (see detail in inset). Figure 3c shows an HRTEM image of several copper oxide nanoparticles; the interplanar distances were calculated as 0.239 and 0.200 nm (inset in Figure 3c), which match the {1,1,1} and {-1,1,2} lattice planes of the monoclinic structure of copper oxide, respectively. Figure 3d shows the SAED pattern indexed by Process Diffraction software [13]; the diffraction rings are associated with the (1,1,0), (1,1,1), (2,0,0), (-1,1,3), (1,1,3), (2,2,0) and (2,2,2) planes of the copper oxide monoclinic structure. The diffraction pattern confirms that the CuONPs possess high crystallinity.

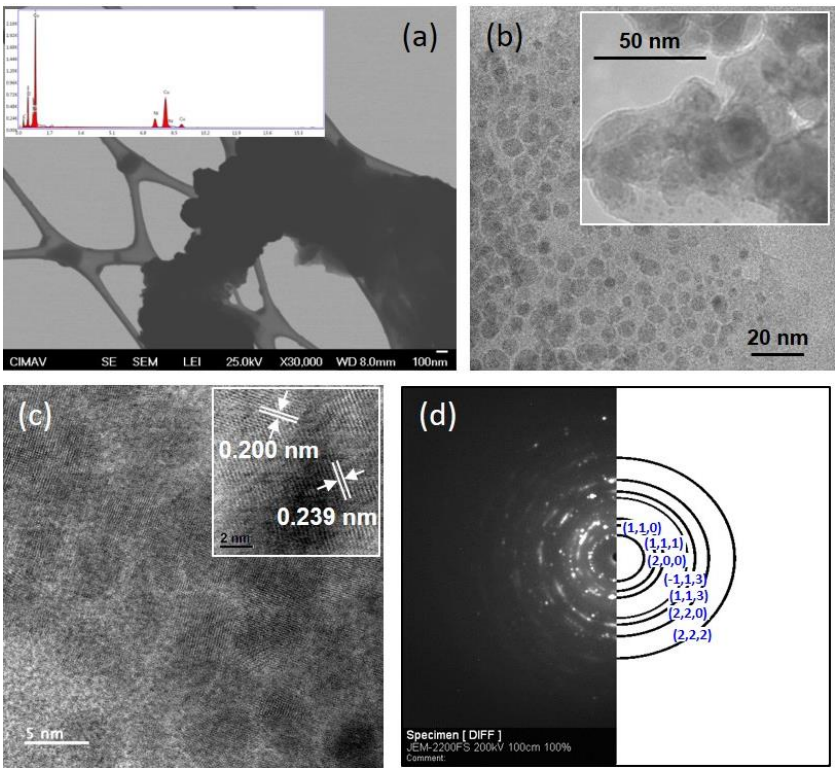

Figure 3. CuO nanoparticles synthesized at pH 10: (a) SEM and EDS analysis, (b) TEM micrograph showing several CuO nanoparticles coated by chitosan, (c) HRTEM image of CuO nanoparticles, (d) indexed SAED pattern.

3.3 Electrochemical study

Figure 4 shows the cyclic voltammograms corresponding to silver (Figure 4a) and copper oxide (Figure 4b) nanoparticles. The oxidation-reduction peaks in Figure 4a are particularly clear. The anodic peak corresponds to the oxidation reaction $Ag^0 \rightarrow Ag^+ + e^-$, while the cathodic peak is related to the opposite reaction, $Ag^+ + e^- \rightarrow Ag^0$. The oxidation peaks are located at 93 and 99 mV for pH 7 and pH 10, respectively. Moreover, reduction peaks appear at -32 and -37 mV, similar to those reported by

Dobre et al. [14], with the difference that previous authors performed cyclic voltammetry using 0.1 M KNO_3 solution at a higher scan rate.

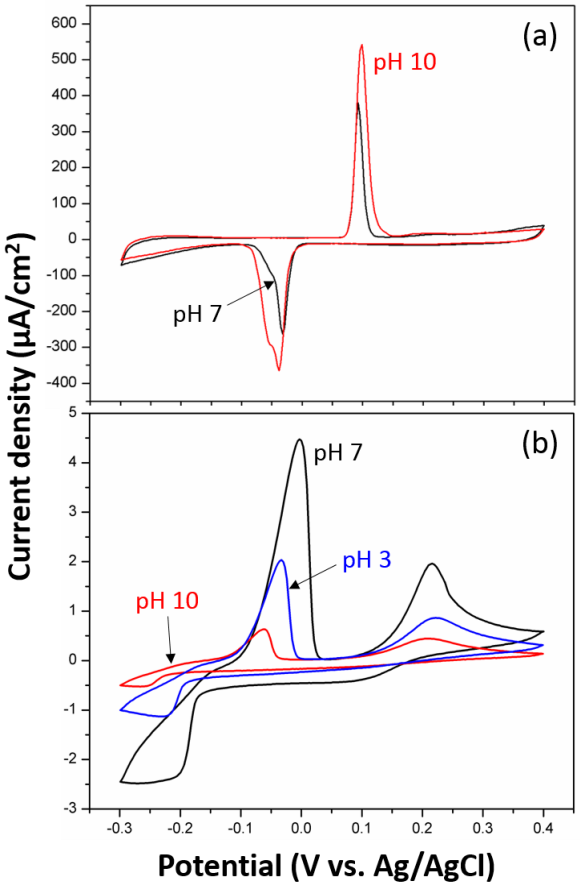

Figure 4. Cyclic voltammetry in 0.3 M HCl at 100 mV/s of (a) AgNPs and (b) CuONPs obtained at different pH values.

The cyclic voltammograms of CuONPs present two distinguishable steps of oxidation-reduction, with the peak values strongly dependent on the synthesis conditions. The first anodic peak, observed at -33, -30 and -63 mV for a pH of 3, 7 and 10, respectively, corresponds to the reaction $Cu^0 \rightarrow Cu^+ + e^-$. The next oxidation peak at 220, 220 and 207 mV is related to the oxidation of Cu^+ ions onto the electrode surface: $Cu^+ \rightarrow Cu^{2+} + e^-$. The sweep of potential in the opposite direction shows a first reduction peak for $Cu^{2+} + e^- \rightarrow Cu^+$, which is not well defined as the other peaks; this effect occurred because Cu^+ was not fully oxidized in the Cu^+/Cu^{2+} oxidation process, which is why Cu^+ ions have a higher concentration in the solution and can be reduced at more negative potentials at approximately -230 mV (Cu^+/Cu^0) [15-16].

3.4 Antimicrobial activity

Table 1 shows the sizes of the bacterial growth inhibition zones of the different AgNP and CuONP solutions; only the CuONP solution at pH 3 exhibited growth inhibition for both bacteria at

different levels (p = 0.025) (Figure 5). The antimicrobial activity of the CuO solution (pH 3) was different from that of an antimicrobial drug against the bacterial species evaluated (p = 0.002). However, the CuONP solution at pH 3 reached a biocidal power similar to that of the conventional drug against *S. aureus* (Table 1).

Table 1. Inhibition zone sizes of Ag and CuO nanoparticle solutions against *E. coli* strains and *S. aureus*.

Nanoparticle solution	Inhibition zone (cm) *	
	E. coli	*S. aureus*
AgNPs at pH 3	0	0
AgNPs at pH 7	0	0
AgNPs at pH 10	0	0
CuONPs at pH 3	0.93± 0.05[b]	1.30± 0.08 cm[a]
CuONPs at pH 7	0	0
CuONPs at pH 10	0	0
Ceftriaxone (30 μl)	1.60 ± 0.05[a]	1.37± 0.05 cm[a]

*Inhibition zone values (cm) are expressed as the median ± standard deviation. Different letters within the columns indicate significance differences at p > 0.05.

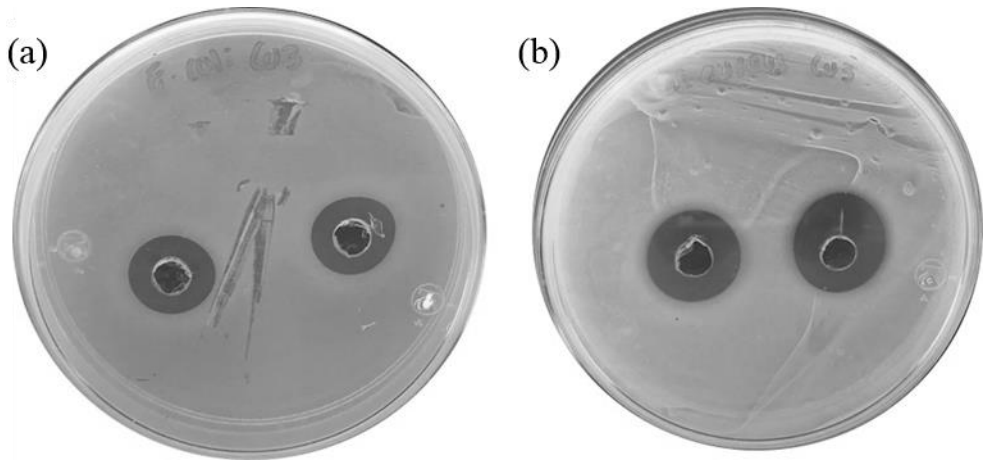

Figure 5. Antimicrobial activity of CuONP solution against (a) *Escherichia coli* ATCC 25922 and (b) *Staphylococcus aureus* ATCC 29213.

These findings suggest the use of CuONPs synthesized in a pH 3 solution as a potential antimicrobial agent. The smaller size and homogeneous morphology of the nanoparticles are consistent with their excellent antimicrobial activity (Table 1). In addition, the CuONP solution reaches inhibition levels similar to those of a conventional antimicrobial drug. Several studies have reported the biocidal efficacy of silver and copper oxide nanoparticles, which is dependent on the synthesis conditions, metal type, concentration, particle size, and stability [17-20]. Furthermore, some researchers have highlighted a better antimicrobial effect of copper oxide nanoparticles on both types of bacteria compared to silver nanoparticles [21, 22]. Although the structures of the bacterial cell walls are

different and the biocidal effect could be dependent on the bacterial species, the CuO nanoparticles have the potential to cause cell death as a consequence of electrostatic interactions between the liberated metal ions and the negatively charged bacterial cell wall, subsequent disruption of the cell membrane and protein denaturation [21].

4. CONCLUSIONS

The present study reported a simple, low-cost and eco-friendly green approach for the synthesis of silver and copper oxide nanoparticles of different sizes depending on the pH used. Optical and structural characterization revealed that the formation of crystalline silver nanoparticles is favorable at high pH (7-10). For the copper oxide nanocrystals, a monoclinic structure can be obtained from pH 3 to pH 10. For both systems, the particle size increased with increasing pH. According to the cyclic voltammetry results, only one redox pair, Ag^0/Ag^+, is present for the silver nanoparticles, while for copper oxide nanoparticles, there are two redox pairs, Cu^0/Cu^+ and Cu^+/Cu^{2+}. Finally, using microbiological tests, it was determined that CuO nanoparticles of smaller size have antibacterial activity against prominent pathogen bacteria, such as *E.coli* and *S.aureus*, with a similar effect to that of a conventional drug, and could therefore potentially be used in medicinal applications.

ACKNOWLEDGEMENTS
The authors thank the Program for the Promotion and Support of Research Projects (PROFAPI) of Universidad Autónoma de Sinaloa (grant PROFAPI-2015/173). The authors also thank Prof. José Ángel López Valenzuela, Prof. Ignacio Contreras Andrade, Prof. Julio Montes Ávila, Ms. José Ernesto Ledezma Sillas, Ms. Jeanett Chavez Ontiveros, Ms. Maritza Castillo Burgos and Ms. Claudia Ochoa Bojórquez for supporting this work with additional facilities.

References

1. J. Conde, G. Doria and P. Baptista, *J. Drug. Deliv.*, 2012 (2012) 1.
2. N. Bellottia, R. Romagnolia, C. Quintero, C. Domínguez-Wong, F. Rui and C. Deyá, *Prog. Org. Coat.*, 86 (2015) 33.
3. S. Paul, C. Pearson, A. Molloy, M. A. Cousins, M. Green, S. Kolliopoulou, P. Dimitrakis, P. Normand, D. Tsoukalas and M. C. Petty, *Nano Lett*., 3 (2003) 533.
4. L. Wang, C. Hu and L. Shao, *Int. J. Nanomedicine*, 12 (2017) 1227.
5. N. Mat Zain, A.G.F.Stapley and G.Sham, *Carbohydr. Polym*., 112 (2014) 195.
6. P. Yugandhar, T. Vasavi, P. Uma, M. Devi and N. Savithramma, *Appl. Nanosci*., 7 (2017) 417.
7. S. Logpriya, V. Bhuvaneshwari, D. Vaidehi, R. P. SenthilKumar, R. S. Nithya Malar, B. PavithraSheetal, R. Amsaveni and M. Kalaiselv, *J. Nanostructure. Chem*., 8 (2018) 301.
8. G. Suriati, M. Mariatti and A. Azizan, *Int. J. Auto. Mech. Eng*., 10 (2014) 1920.
9. O. Velgosová, A. Mražíková and R. Marcinčáková, *Mater. Lett*., 180 (2016) 336.
10. J.I. Hussain, S. Kumar, A.A. Hashmi and Z. Khan, *Adv. Mat. Lett*., 2 (2011) 188.
11. S.T. Fardood and A. Ramazani, *J. Nanostruct*., 6 (2016) 160.
12. S. Jillani, M. Jelani, N. Hassan, S. Ahmad and M. Hafeez, *Mater. Res. Express*, 5 (2018) 045006.
13. J.L. Lábár, *Ultramicroscopy*, 103 (2005) 237.
14. N. Dobre, F. Golgovici, L. Anicai and M. Buda, *Rev. Chim*., 65 (2014) 578.

15. V. Prakash, R.K. Diwan and V.K. Niyogi, *Indian J. Pure & Appl. Phys*., 53 (2014) 753.
16. Md. Sohel, M. Arifur and A. M. Shafiqul ,*Pak. J. Anal. Environ. Chem*., 15 (2014) 13.
17. L.L. Duffy, M. J. Osmond-McLeod, J. Judy and T. King, *Food Control*, 92 (2018) 293.
18. P. Harikumar and A. Aravind, *Int. J. Sci.*, 5 (2016) 83.
19. X. Hong, J. Wen and Y. Hu, Environ. Sci. Pollut. *Res. Int*., 23 (2016) 4489.
20. S. Pal, S., Y.K. Tak and J.M. Song, *Appl. Environ. Microbiol*., 73 (2007) 1712.
21. S. Mahmoodi, A. Elmi and S. Hallaj-Nezhad, *J. Mol. Pharm. Org. Process. Res*, 6 (2018) 1000140.
22. P.A. B.R. Bhutkar, Y.D. Dange and S.V. Kharat ,*J. Nanomed. Nanotechnol*., 7 (2016) 1000353.